PAPER

CrossMark
click for updates

Bottom-up and top-down methods to improve catalytic reactivity for photocatalytic production of hydrogen peroxide using a Ru-complex and water oxidation catalysts†

Yusuke Isaka,[a] Satoshi Kato,[a] Dachao Hong,[a] Tomoyoshi Suenobu,[a] Yusuke Yamada[a] and Shunichi Fukuzumi*[abc]

Hydrogen peroxide (H_2O_2) was produced from water and dioxygen using $[Ru^{II}(Me_2phen)_3]^{2+}$ (Me_2phen = 4,7-dimethyl-1,10-phenanthroline) as a photocatalyst and $[Ir(Cp*)(H_2O)_3]^{2+}$ ($Cp*$ = η^5-pentamethylcyclopentadienyl) as a precursor of a water oxidation catalyst in the presence of Sc^{3+} in water under visible light irradiation. TEM and XPS measurements of residues in the resulting solution after the photocatalytic production of H_2O_2 indicated that $[Ir(Cp*)(H_2O)_3]^{2+}$ was converted to $Ir(OH)_3$ nanoparticles, which are actual catalytic species. The $Ir(OH)_3$ nanoparticles produced *in situ* during the photocatalytic production of H_2O_2 were smaller in size than those prepared independently from hydrogen hexachloroiridiate (H_2IrCl_6), and exhibited higher catalytic reactivity for the photocatalytic production of H_2O_2. The photocatalytic production of H_2O_2 from water and dioxygen was also made possible when $Ir(OH)_3$ nanoparticles were replaced by nickel ferrite ($NiFe_2O_4$) nanoparticles, which are composed of more earth abundant metals than iridium. The size of $NiFe_2O_4$ nanoparticles became smaller during the photocatalytic production of H_2O_2 to exhibit higher catalytic reactivity in the second run as compared with that in the first run. $NiFe_2O_4$ nanoparticles obtained by the treatment of $NiFe_2O_4$ in an aqueous solution of Sc^{3+} exhibited 33-times higher catalytic reactivity in H_2O_2-production rates than the as-prepared $NiFe_2O_4$. Thus, both the bottom-up method starting from a molecular complex $[Ir(Cp*)(H_2O)_3]^{2+}$ and the top-down method starting from as-prepared $NiFe_2O_4$ to obtain nanoparticles with smaller size resulted in the improvement of the catalytic reactivity for the photocatalytic production of H_2O_2 from water and dioxygen.

Introduction

The rapid and unsustainable use of fossil fuels has led to increased attention paid to the development of zero-carbon emission fuels, particularly hydrogen, utilizing renewable energy sources.[1–7] Solar energy is obviously the most abundant among the renewable energy sources under consideration. Thus, extensive efforts have been devoted to producing

[a]*Department of Material and Life Science, Graduate School of Engineering, Osaka University, ALCA, SENTAN, Japan Science and Technology Agency (JST), Suita, Osaka 565-0871, Japan. E-mail: fukuzumi@chem.eng.osaka-u.ac.jp*

[b]*Faculty of Science and Engineering, Meijo University, ALCA, SENTAN, Japan Science and Technology Agency (JST), Nagoya, Aichi 468-0073, Japan*

[c]*Department of Bioinspired Science, Ewha Womans University, Seoul 120-750, Korea*

† Electronic supplementary information (ESI) available: Experimental section, time courses of H_2O_2 production under different conditions (Fig. S1, S2, S14–S17), TEM images (Fig. S3, S5 and S13), X-ray photoelectron spectra of $Ir(OH)_3$ (Fig. S4), time course of H_2O_2 decomposition in the presence of $NiFe_2O_4$ (Fig. S6), DLS data (Fig. S7–S10), powder XRD patterns (Fig. S11), UV-Vis spectra (Fig. S12) and appendix for the derivation of specific surface area of particles. See DOI: 10.1039/c5ta02446c

hydrogen by water splitting (eqn (1)), which is highly endergonic with a free energy change of $\Delta G° = 474$ kJ mol^{-1}, which is provided by solar energy.[8–12] In this case, however, a method for separating the simultaneously produced H_2 and O_2 remains to be developed to avoid possible explosion.[13] In addition, the storage of hydrogen at reasonable energy density poses a technical and economical challenge due to its low volumetric energy.[14,15]

$$2H_2O \rightarrow 2H_2 + O_2 \qquad \Delta G° = 474 \text{ kJ mol}^{-1} \quad (1)$$

In contrast to hydrogen, hydrogen peroxide (H_2O_2) is miscible in water, and therefore it can be an ideal energy carrier alternative to hydrogen, because H_2O_2 can be used as a fuel for one-compartment fuel cells.[16–23] The output potential of a H_2O_2 fuel cell theoretically achievable is 1.09 V, which is comparable with that of a hydrogen fuel cell (1.23 V).[16,17] Thus, a combination of H_2O_2 production using solar energy and power generation with an H_2O_2 fuel cell provides an ideally sustainable solar fuel.[16,17] It is desired to produce H_2O_2 from H_2O and O_2 (eqn (2)),

12404 | *J. Mater. Chem. A*, 2015, **3**, 12404–12412

This journal is © The Royal Society of Chemistry 2015

which is highly endergonic with the free energy change of $\Delta G^\circ = 210$ kJ mol^{-1}, by using solar energy.[16,17]

$$2H_2O + O_2 \rightarrow 2H_2O_2 \qquad \Delta G^\circ = 210 \text{ kJ mol}^{-1} \quad (2)$$

We have recently reported the photocatalytic production of H_2O_2 from H_2O and O_2 by combining the photoreduction of O_2 with a Ru-complex photosensitiser and water oxidation with Ir(OH)$_3$ nanoparticles as water oxidation catalysts (WOCs) in the presence of Sc^{3+} in water under visible light irradiation.[24] In order to improve the photocatalytic reactivity of H_2O_2 production from H_2O and O_2, it is required to employ more efficient WOCs. Extensive efforts have so far been devoted to developing efficient WOCs using transition metal complexes.[25–45] In particular, a series of mononuclear iridium(III) complexes with the η^5-pentamethylcyclopentadienyl ligand (Cp*) have been reported to act as efficient WOCs, which are more active than ruthenium complexes.[46–49] The Cp* ligand is expected to provide electron rich circumstances useful to stabilise reaction intermediates possessing a high-valent oxidation state in catalytic water oxidation by cerium ammonium nitrate, $(NH_4)_2[Ce(NO_3)_6]$, (CAN).[46–49] Under the conditions of catalytic water oxidation by CAN, however, the Cp* ligand of Ir complexes has been reported to be oxidised to produce IrO$_2$ or Ir(OH)$_3$ nanoparticles, which act as the actual reactive catalyst for water oxidation.[50–54] IrO$_2$ or Ir(OH)$_3$ nanoparticles have been reported to be more active than conventional IrO$_2$ prepared from H_2IrCl_6.[55–61] Thus, *in situ* formation of a WOC provides a useful way to improve the catalytic reactivity for water oxidation.

We report herein the photocatalytic production of H_2O_2 from H_2O and O_2 using an Ir complex, [Ir(Cp*)(H$_2$O)$_3$]$^{2+}$, as a precursor of a water oxidation catalyst and [Ru^{II}(Me$_2$phen)$_3$]$^{2+}$ (Me$_2$phen = 4,7-dimethyl-1,10-phenanthroline) as a homogeneous photocatalyst in the presence of Sc^{3+} in water. The characterisation of the catalytically active species has revealed that [Ir(Cp*)(H$_2$O)$_3$]$^{2+}$ is converted to Ir(OH)$_3$ nanoparticles, which exhibit high catalytic reactivity for photocatalytic water oxidation. A synthetic strategy for such Ir(OH)$_3$ nanoparticles from H_2IrCl_6 has not yet been established. Because Ir is a noble metal with limited natural supplies, it is desired to replace the noble metal in WOCs by more earth-abundant metals such as Fe and Ni. In this context, we have also employed nanoparticles composed of earth abundant nickel and iron (NiFe$_2$O$_4$) instead of the Ir complex as a water oxidation catalyst for the photocatalytic production of H_2O_2. During the reaction, NiFe$_2$O$_4$ nanoparticles were formed from the corresponding as-prepared NiFe$_2$O$_4$. The effect of reaction conditions on the reactivity of the therein-formed nanoparticles from the Ir complex or NiFe$_2$O$_4$ is discussed in this paper.

Results and discussion

Photocatalytic production of hydrogen peroxide with an iridium complex precatalyst

The photocatalytic production of H_2O_2 was performed using [Ru^{II}(Me$_2$phen)$_3$]$^{2+}$ as a photocatalyst for the two-electron reduction of O_2 and various Ir compounds as WOCs in the

presence of Sc^{3+} ions in distilled water as shown in Fig. 1a. Sc^{3+} ions were reported to prohibit back electron transfer from $O_2^{\bullet-}$ to [Ru^{III}(Me$_2$phen)$_3$]$^{3+}$, which is formed after photoinduced electron transfer to O_2 from an excited state of [Ru^{II}(Me$_2$phen)$_3$]$^{2+}$ (*vide infra*).[24] The initial rate of H_2O_2 production using [Ir(Cp*)(H$_2$O)$_3$]$^{2+}$ (red squares in Fig. 1a) was 4.5 times faster than that using Ir(OH)$_3$ nanoparticles (blue circles in Fig. 1a) prepared from H_2IrCl_6 with the same amount of Ir.[54] The rate of H_2O_2 production using [Ir(Cp*)(H$_2$O)$_3$]$^{2+}$ was 4.4 times and 2.8 times faster than those using Ir(SO$_4$)$_2$ and [Ir(Cp*)((OH)$_2$-bpy)(H$_2$O)]$^{2+}$ ((OH)$_2$bpy = 4,4′–(OH)$_2$–2,2′-bipyridine), respectively. [Ir(Cp*)(H$_2$O)$_3$]$^{2+}$ had higher reactivity than Co complexes and Co ions, which have been reported to act as highly active WOCs, as shown in Fig. 1b.[62,63] The quantum efficiency determined by using monochromatised light (450 nm) and the solar energy conversion efficiency of the production of H_2O_2 were determined to be 7.1% and 0.063%, respectively (Fig. S1 and S2†). The sigmoidal behaviour in the initial stage of H_2O_2 production with [Ir(Cp*)(H$_2$O)$_3$]$^{2+}$ (Fig. 2, green) indicates that [Ir(Cp*)(H$_2$O)$_3$]$^{2+}$ acts as a precatalyst to produce catalytically more active species during the photocatalytic production of H_2O_2.

The sigmoidal behaviour was more pronounced when the photocatalytic production of H_2O_2 was performed at 278 K as shown in Fig. 2 (red circles), where the results at higher temperatures are compared. The initial rate of H_2O_2 production increases with increasing temperature (Fig. 2), but the maximum H_2O_2 concentration decreased because of the enhanced decomposition of H_2O_2.

The formation of nanoparticles was observed by transmission electron microscopy (TEM) measurements. TEM images of the particles (Fig. S3†) showed that the diameters of the particles increased by extending the reaction time. The formation of nanoparticles was also confirmed by dynamic light scattering (DLS) measurements as shown in Fig. 3. The size of nanoparticles formed after 12 h photoirradiation at 278 K was 21 nm, whereas the size increased to 240 nm after 36 h
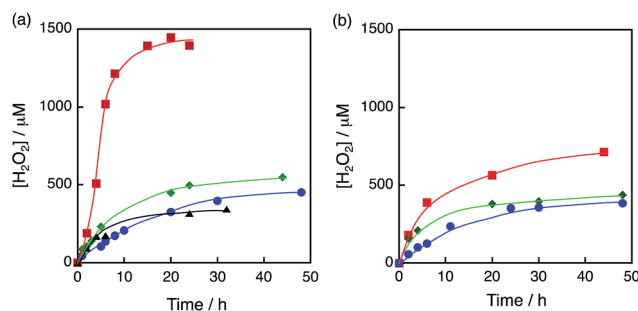

Fig. 1 Time courses of H_2O_2 production under visible light ($\lambda > 420$ nm) irradiation of [Ru^{II}(Me$_2$phen)$_3$]$^{2+}$ (20 μM) in the presence of Sc^{3+} (100 mM) in O$_2$-saturated H_2O (3.0 mL, [O$_2$] = 1.2 mM) containing (a) various Ir compounds, [Ir(Cp*)(H$_2$O)$_3$]$^{2+}$ (red squares), [Ir(Cp*)((OH)$_2$-bpy)(H$_2$O)]$^{2+}$ (green diamonds), Ir(OH)$_3$ (blue circles) and Ir(SO$_4$) (black triangles), where Ir content: 100 μM and (b) various Co compounds, [Co(Cp*)(bpy)(H$_2$O)]$^{2+}$ (red squares), [Co(Cp*)(H$_2$O)$_3$]$^{2+}$ (green diamonds) and Co(NO$_3$)$_3$ (blue circles), where Co content: 100 μM at 298 K.

This journal is © The Royal Society of Chemistry 2015

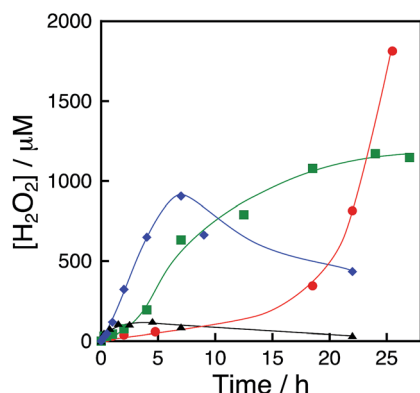*J. Mater. Chem. A*, 2015, **3**, 12404–12412 | **12405**

Fig. 2 Time courses of H_2O_2 production under visible light ($\lambda > 420$ nm) irradiation of $[Ru^{II}(Me_2phen)_3]^{2+}$ (20 μM) in the presence of $[Ir(Cp^*)(H_2O)_3]^{2+}$ (100 μM) and Sc^{3+} (100 mM) in an O_2-saturated aqueous solution (3.0 mL) at 333 K (black triangles), 313 K (blue diamonds), 293 K (green squares) and 278 K (red circles).
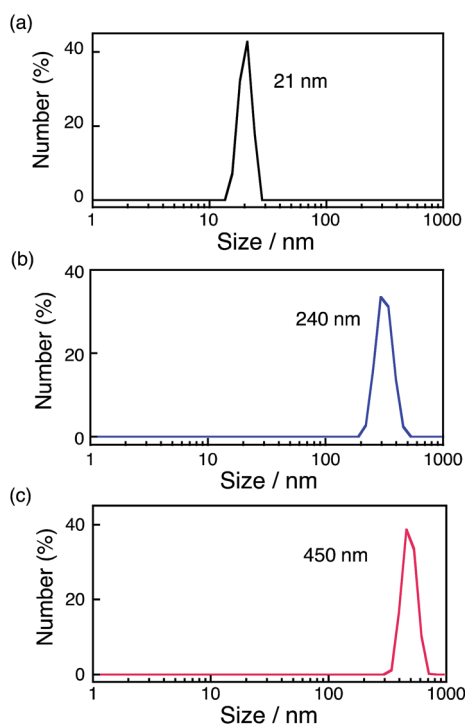

Fig. 3 Size distributions of the particles obtained by DLS measurements. The particles were formed under visible light ($\lambda > 420$ nm) irradiation of $[Ru^{II}(Me_2phen)_3]^{2+}$ (20 μM) in the presence of $[Ir(Cp^*)(H_2O)_3]^{2+}$ (100 μM) and Sc^{3+} (100 mM) in an O_2-saturated aqueous solution (3.0 mL) at 298 K for (a) 12 h, (b) 36 h and (c) at 333 K for 12 h.

photoirradiation. Large-sized particles (450 nm) were obtained after 12 h photoirradiation at 333 K. Thus, the size of the particles depends on the photoirradiation time and temperature. During photocatalytic H_2O_2 production, the size of the nanoparticles (21 nm) increases to 240 nm after 36 h (Fig. 3a and b) and the rate of the reaction decreases (Fig. 2, green line) under irradiation of visible light at room temperature. The

deceleration of the reaction rate may be ascribed to the decrease in the surface area of the nanoparticles with increasing the size of the nanoparticles. $[Ir(Cp^*)(H_2O)_3]^{2+}$ has been reported to be efficiently oxidised by CAN, and TG/DTA and XPS measurements of nanoparticles produced after the water oxidation suggested that the nanoparticles were composed of $Ir(OH)_3$.[61] XPS measurements of the nanoparticles centrifugally recovered from the reaction solution after the H_2O_2 production reaction were performed for the energy regions of Ir 4f, O 1s and C 1s with reference to commercially available IrO_2 (Fig. S4†), which suggested that the formed nanoparticles are also composed of $Ir(OH)_3$. Since the binding energy of Ir $4f_{5/2}$ reflects the valence of Ir ions, the value was determined to be 61.9 eV for $Ir(OH)_3$ nanoparticles, which is close to the reported value for Ir^{III} (62.0 eV).[62] These values were significantly different from those for Ir^0 (61.0 eV) or Ir^{IV} (63.7 eV).[58,62–67] The binding energy for O 1s of $Ir(OH)_3$ nanoparticles (531.9 eV) shifted from that of IrO_2 (530.2 eV) due to the OH moiety as reported previously.[54] TEM images of $Ir(OH)_3$ nanoparticles revealed that the size of $Ir(OH)_3$ nanoparticles (10–20 nm) derived from $[Ir(Cp^*)(H_2O)_3]^{2+}$ was
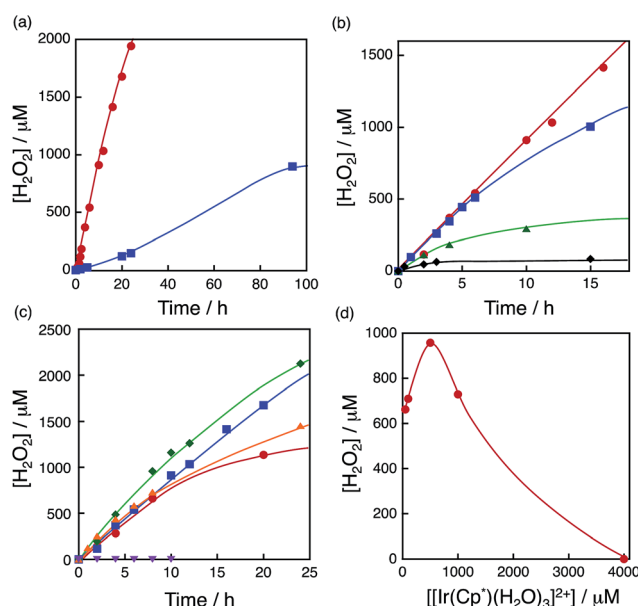

Fig. 4 (a) Time courses of H_2O_2 production at different concentrations of $[Ru^{II}(Me_2phen)_3]^{2+}$ [20 μM (red circles) and 1.0 μM (blue squares)] under irradiation of $[Ru^{II}(Me_2phen)_3]^{2+}$ with visible light ($\lambda > 420$ nm) in the presence of $[Ir(Cp^*)(H_2O)_3]^{2+}$ (100 μM) and Sc^{3+} (100 mM) in O_2-saturated H_2O (3.0 mL, $[O_2] = 1.2$ mM) at 298 K. (b) Time courses of H_2O_2 production at different concentrations of Sc^{3+} [0 mM (black diamonds), 1.0 mM (green triangles), 10 mM (blue squares) and 100 mM (red circles)] under irradiation of $[Ru^{II}(Me_2phen)_3]^{2+}$ (20 μM) with visible light ($\lambda > 420$ nm) in the presence of $[Ir(Cp^*)(H_2O)_3]^{2+}$ (100 μM) in O_2-saturated H_2O (3.0 mL, $[O_2] = 1.2$ mM) at 298 K. (c) Time courses of H_2O_2 production at different concentrations of $[Ir(Cp^*)(H_2O)_3]^{2+}$ [50 μM (red circles), 100 μM (blue squares), 500 μM (green diamonds), 1000 μM (orange triangles) and 4000 μM (purple inverse triangles)] at 298 K. (d) Plot of the amount of H_2O_2 production after 8 h vs. the concentration of $[Ir(Cp^*)(H_2O)_3]^{2+}$ under irradiation of $[Ru^{II}(Me_2phen)_3]^{2+}$ (20 μM) with visible light ($\lambda > 420$ nm) in the presence of Sc^{3+} (100 mM) in O_2-saturated H_2O (3.0 mL, $[O_2] = 1.2$ mM) at 298 K.

12406 | J. Mater. Chem. A, 2015, **3**, 12404–12412

This journal is © The Royal Society of Chemistry 2015

smaller than that of $Ir(OH)_3$ (30–100 nm) derived from H_2IrCl_6 (Fig. S5†). The higher catalytic reactivity of $Ir(OH)_3$ nanoparticles derived from $[Ir(Cp^*)(H_2O)_3]^{2+}$ may result from the smaller size of the nanoparticles as compared with those derived from H_2IrCl_6.

The dependence of photocatalytic reactivity for H_2O_2 production on the concentration of $[Ru^{II}(Me_2phen)_3]^{2+}$ was examined as shown in Fig. 4a. The photocatalytic reactivity decreased with decreasing the concentration of $[Ru^{II}(Me_2phen)_3]^{2+}$, however, the highest TON based on $[Ru^{II}(Me_2phen)_3]^{2+}$ was determined to be 898 after 94 h photoirradiation when the concentration of $[Ru^{II}(Me_2phen)_3]^{2+}$ was reduced to 1.0 μM, which is much higher than that reported for the photocatalytic H_2O_2 production using $Ir(OH)_3$ as a WOC (307).[24]

The dependence of photocatalytic reactivity for H_2O_2 production on the concentration of Sc^{3+} was also examined as shown in Fig. 4b. The photocatalytic reactivity increased with increasing the concentration of Sc^{3+}. This is because Sc^{3+} inhibits back electron transfer from $O_2^{•-}$ to $[Ru^{III}(Me_2phen)_3]^{3+}$, which is generated by photoinduced electron transfer from the excited state of $[Ru^{II}(Me_2phen)_3]^{2+}$ to O_2 as reported previously.[24]

The dependence of photocatalytic reactivity of H_2O_2 production on the concentration of $[Ir(Cp^*)(H_2O)_3]^{2+}$ is shown in Fig. 4c. The highest TON based on $[Ir(Cp^*)(H_2O)_3]^{2+}$ was determined to be 23 after 20 h photoirradiation when 50 μM of $[Ir(Cp^*)(H_2O)_3]^{2+}$ was employed in the photocatalytic H_2O_2 production. The photocatalytic reactivity increased with increasing concentration of $[Ir(Cp^*)(H_2O)_3]^{2+}$, but it decreased through the maximum value with further increase in the concentration of $[Ir(Cp^*)(H_2O)_3]^{2+}$ as shown in Fig. 4d. The decrease in the rate of H_2O_2 production may result from the catalytic decomposition of H_2O_2 with $[Ir(Cp^*)(H_2O)_3]^{2+}$ as shown in Fig. 5a. When a high concentration of $[Ir(Cp^*)(H_2O)_3]^{2+}$ (e.g., 1000 μM) was employed in the photocatalytic production of H_2O_2, a part of $[Ir(Cp^*)(H_2O)_3]^{2+}$ may remain without the full conversion to $Ir(OH)_3$ nanoparticles. When a low concentration

of $[Ir(Cp^*)(H_2O)_3]^{2+}$ was employed, all of the $[Ir(Cp^*)(H_2O)_3]^{2+}$ may be oxidised to produce $Ir(OH)_3$ nanoparticles during the photocatalytic reaction. The formed $Ir(OH)_3$ nanoparticles are less reactive toward H_2O_2 decomposition as compared to $[Ir(Cp^*)(H_2O)_3]^{2+}$ (Fig. 5). The conversion of $[Ir(Cp^*)(H_2O)_3]^{2+}$ to $Ir(OH)_3$ during the photocatalytic production of H_2O_2 may be associated with the oxidation of the Cp^* ligand by O_2. The full oxidation of Cp^* is expected to produce 10 equivalents of CO_2 and 8 equivalents of H_2O_2 (eqn (3)). During the photocatalytic production of H_2O_2, CO_2 evolution was observed as shown in Fig. 6a. However, the yield of CO_2 based on eqn (3) is only 1%. Thus, the Cp^* ligand is only partially oxidised to CO_2. The amount of H_2O_2 that is expected to be produced from Cp^* calculated based on eqn (3) [Fig. 6b (blue line)] was negligible as compared with the observed amount of H_2O_2 in Fig. 6b (red line). These results indicate that H_2O_2 was produced by using H_2O as an electron source.

$$C_{10}H_{15}^- + 18O_2 + H^+ \rightarrow 10CO_2 + 8H_2O_2 \tag{3}$$
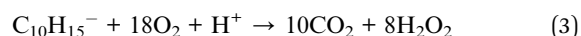
Photocatalytic production of hydrogen peroxide with $NiFe_2O_4$ nanoparticles

The catalytic reactivity of nickel ferrite ($NiFe_2O_4$) for water oxidation has been reported to be comparable to that of a catalyst containing Ir, Ru or Co in terms of the oxygen yield and oxygen-evolving rate under ambient reaction conditions.[67]

Because $NiFe_2O_4$ is composed of much more earth-abundant metals than Ir, $NiFe_2O_4$ was employed as a WOC for the photocatalytic production of H_2O_2 with $[Ru^{II}(Me_2phen)_3]^{2+}$ in the presence of Sc^{3+} in water. The overall photocatalytic cycle for H_2O_2 production is depicted in Scheme 1. Photoinduced electron transfer from the excited state of $[Ru^{II}(Me_2phen)_3]^{2+}$ to O_2 results in the formation of H_2O_2 and $[Ru^{III}(Me_2phen)_3]^{3+}$ via the oxidation of $NiFe_2O_4$, which oxidises water to form O_2 and $[Ru^{II}(Me_2phen)_3]^{2+}$. Back electron transfer from $O_2^{•-}$ to
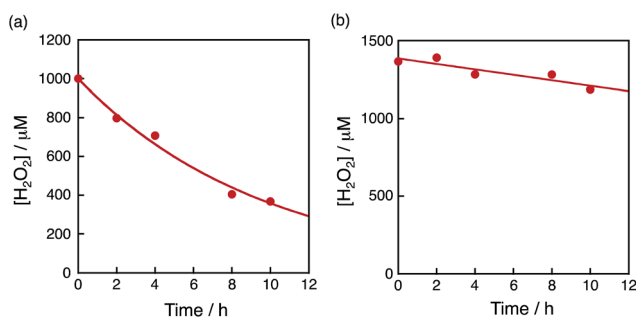
Fig. 5   Time course of the concentration of H_2O_2 in the presence of (a) $[Ir(Cp^*)(H_2O)_3]^{2+}$ (100 μM) and (b) the $Ir(OH)_3$ nanoparticles in H_2O (3.0 mL) at 298 K containing H_2O_2 and Sc^{3+} (100 mM) under dark conditions. The $Ir(OH)_3$ nanoparticles used were formed after 16 h photoirradiation of $[Ru^{II}(Me_2phen)_3]^{2+}$ (20 μM) with visible light (λ > 420 nm) in the presence of $[Ir(Cp^*)(H_2O)_3]^{2+}$ (100 μM) and Sc^{3+} (100 mM) in O_2-saturated H_2O (3.0 mL, $[O_2]$ = 1.2 mM) at 298 K and the resulting aqueous suspension was used as is for the measurements.
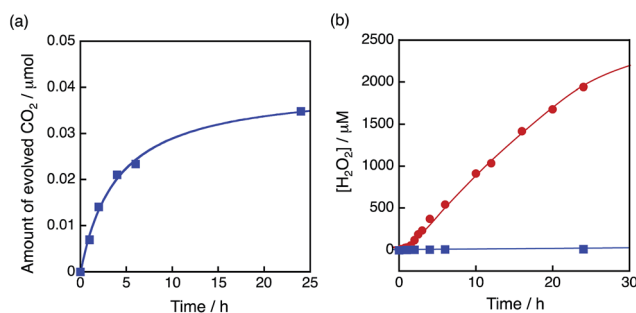
Fig. 6   (a) Time course of CO_2 evolution at 298 K under visible light (λ > 420 nm) irradiation of $[Ru^{II}(Me_2phen)_3]^{2+}$ (20 μM) in the presence of Sc^{3+} (100 mM) in O_2-saturated H_2O (3.0 mL, $[O_2]$ = 1.2 mM) containing $[Ir(Cp^*)(H_2O)_3]^{2+}$ (100 μM). (b) Time course of H_2O_2 production at 298 K under visible light (λ > 420 nm) irradiation of $[Ru^{II}(Me_2phen)_3]^{2+}$ (20 μM) in the presence of Sc^{3+} (100 mM) in O_2-saturated H_2O (3.0 mL, $[O_2]$ = 1.2 mM) containing $[Ir(Cp^*)(H_2O)_3]^{2+}$ (100 μM) (red circles). Blue squares are the time course of H_2O_2 production expected from the amount of evolved CO_2 based on eqn (3).
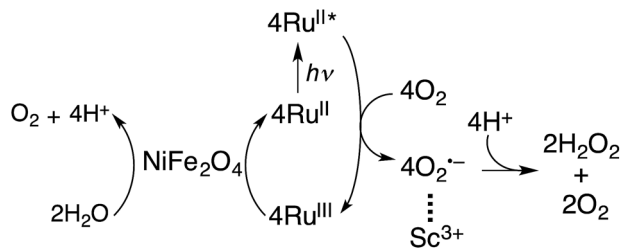
Scheme 1 Overall photocatalytic cycle for H_2O_2 production.

$[Ru^{III}(Me_2phen)_3]^{3+}$ and the decomposition of H_2O_2 by $NiFe_2O_4$ are retarded in the presence of Sc^{3+} (*vide supra*, Fig. S6†).[24]

The photocatalytic production of H_2O_2 was performed using $[Ru^{II}(Me_2phen)_3]^{2+}$ as a photosensitiser and $NiFe_2O_4$ as a WOC (Fig. 7a), which exhibited an induction period at the initial reaction time (black line in Fig. 7b). From the resulting solution, $NiFe_2O_4$ nanoparticles were recovered by centrifugation after 12 h photoirradiation and reused as WOCs. With the use of recovered $NiFe_2O_4$ as WOCs, the induction period was not observed (blue line in Fig. 7b). The diameter of nanoparticles measured by DLS decreased from 1300 nm to 620 nm after 12 h reaction as shown in Fig. 7c, suggesting that the induction period originates from the decrease in the diameter during the reaction.

In order to determine the conditions necessary for the size change of as-prepared $NiFe_2O_4$, DLS measurements of $NiFe_2O_4$ in an aqueous solution containing Sc^{3+} (100 mM) were performed under dark (Fig. S7†). The diameter of $NiFe_2O_4$ particles decreased to 710 nm, which is in good agreement with the size

observed for the particles in the reaction suspension, although the rate of the size change was significantly reduced to 1/20 of that under photoirradiation. This result indicates that the rate of the size change was accelerated with photoirradiation. Then, the size change of $NiFe_2O_4$ was also examined in an aqueous HNO_3 (1.0 M) solution (Fig. S8†) because Fe and Ni ions can be soluble in highly acidic solutions. However, the deceleration of the rate of the size change was also observed in the HNO_3 solution under dark conditions, as the diameter of $NiFe_2O_4$ did not change even after 24 h under dark conditions (Fig. S9†). These results indicate that the presence of Sc^{3+} is necessary for the size change, thus, the dependence of the rate of the size change on the concentration of Sc^{3+} ranging from 0.1 to 100 mM was examined under room light at 353 K. The fastest size-decreasing rate was observed for an aqueous solution containing 10 mM of Sc^{3+} (Fig. S10†). Under these conditions, the size of formed nanoparticles became as small as 91 nm after 12 h (Fig. 8).

The nanoparticles were characterised by powder XRD to confirm that they kept the ferrite structure (Fig. S11†). It was also confirmed that the as-prepared $NiFe_2O_4$ was not dissolved to yield Fe ions. The addition of 1,10-phenanthroline (phen) and the reduced form of β-nicotinamide adenine dinucleotide disodium salt hydrate (NADH) as a reductant to the supernatant containing Fe ions produces $[Fe^{II}(phen)_3]^{2+}$, which has strong absorption in the visible region ($\lambda_{max} = 508$ nm, $\varepsilon = 1.1 \times 10^4$ M^{-1} cm^{-1}) and therefore is easily detected (Fig. S12†). It was also supported by the fact that $NiFe_2O_4$ nanoparticles used in the reaction solution were recovered by centrifugation in high
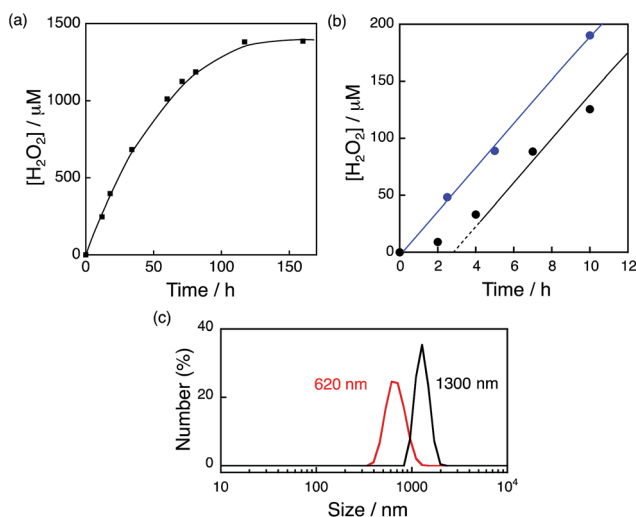

Fig. 8 Size distributions of $NiFe_2O_4$ nanoparticles determined by DLS measurements for an aqueous suspension containing as-prepared $NiFe_2O_4$ (0.17 g L^{-1}) (black) and an aqueous suspension containing $NiFe_2O_4$ particles (0.17 g L^{-1}) and Sc^{3+} (10 mM) exposed to room light for 3 h (green), 6 h (blue) and 12 h (red) at 353 K.

Fig. 7 (a) Time course of H_2O_2 production in the presence of $NiFe_2O_4$ (0.17 g L^{-1}) and Sc^{3+} (100 mM) under visible light irradiation ($\lambda > 420$ nm) of $[Ru^{II}(Me_2phen)_3]^{2+}$ (200 μM) in O_2-saturated H_2O (3.0 mL, $[O_2]$ = 1.2 mM). (b) Initial period of the plot in (a) (black) and the time course of H_2O_2 production in the presence of $NiFe_2O_4$ recovered from the reaction solution after 12 h of visible light ($\lambda > 420$ nm) irradiation under the same conditions as in (a) (blue). (c) Size distributions of $NiFe_2O_4$ particles determined by DLS in the reaction solution before (black) and after (red) 12 h reaction.
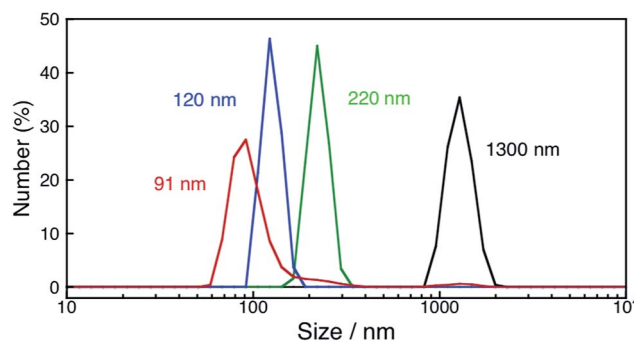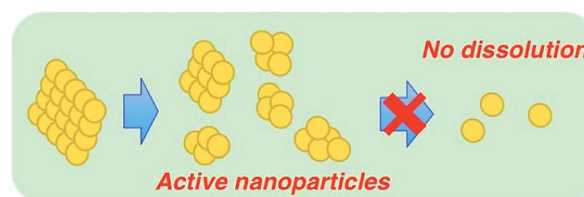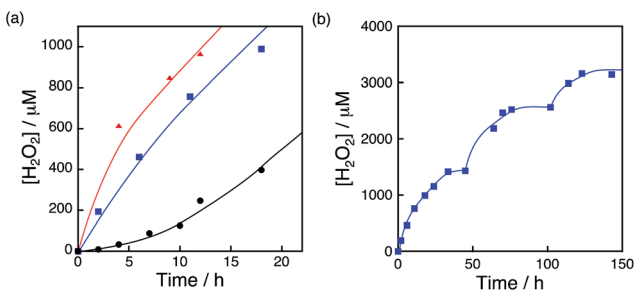

Scheme 2 Mechanism of $NiFe_2O_4$ nanoparticle formation.

12408 | *J. Mater. Chem. A*, 2015, **3**, 12404–12412

This journal is © The Royal Society of Chemistry 2015

Fig. 9 (a) Time courses of H_2O_2 production under visible light irradiation ($\lambda > 420$ nm) of $[Ru^{II}(Me_2phen)_3]^{2+}$ (200 µM) in the presence of Sc^{3+} (100 mM) and $NiFe_2O_4$ (0.17 g L^{-1}) with diameters of 1300 nm (black circles), 120 nm (blue squares) and 91 nm (red triangles) in O_2-saturated H_2O (3.0 mL, $[O_2] = 1.2$ mM). (b) Time course of H_2O_2 production in the presence of $NiFe_2O_4$ (0.17 g L^{-1}) and Sc^{3+} (100 mM) under visible light irradiation ($\lambda > 420$ nm) of $[Ru^{II}(Me_2phen)_3]^{2+}$ (200 µM) in O_2-saturated H_2O (3.0 mL, $[O_2] = 1.2$ mM). $[Ru^{II}(Me_2phen)_3]^{2+}$ was added twice to the reaction suspension at 50 h and 100 h during photoirradiation. The amount of $[Ru^{II}(Me_2phen)_3]^{2+}$ added each time at 50 h and 100 h to the reaction suspension was calculated in terms of the concentration increase of 200 µM.

yield (87%). TEM images of $NiFe_2O_4$ particles manifested that the as-prepared $NiFe_2O_4$ has the form of aggregated smaller primary particles (Fig. S13†). The nanoparticles were formed by the dissociation of small particles that consist of a few primary particles as depicted in Scheme 2.

The photocatalytic production of H_2O_2 was performed using $NiFe_2O_4$ nanoparticles as the WOCs in the presence of $[Ru^{II}(Me_2phen)_3]^{2+}$ and Sc^{3+} under visible light irradiation ($\lambda > 420$ nm) (Fig. 9a and S14†). The quantum efficiency determined by using monochromatised light (450 nm) and solar energy conversion efficiency were determined to be 2.7% and 0.088%, respectively, using $NiFe_2O_4$ nanoparticles with a diameter of

90 nm (Fig. S15 and S16†). To reuse the nanoparticles after H_2O_2 production ceased, an aliquot of an aqueous solution containing a high concentration of $[Ru^{II}(Me_2phen)_3]^{2+}$ was added to the reaction suspension repeatedly, in which the amount of $[Ru^{II}(Me_2phen)_3]^{2+}$ added to the starting suspension at each run was calculated in terms of the concentration increase of 200 µM. The concentration of H_2O_2 in the resulting suspension increased to be as high as 3.3 mM, ensuring the high stability of the nanoparticles as WOCs (Fig. 9b). The initial rate of H_2O_2 production was accelerated 22 times and 33 times when using $NiFe_2O_4$ nanoparticles with diameters of 120 nm and 91 nm, respectively, as compared to the as-prepared $NiFe_2O_4$ with a diameter of 1300 nm (Fig. 9a). This increase in reactivity could be due to a simple increase in the surface area, therefore, surface areas for nanoparticles were estimated from the respective diameters by eqn (S5)† and compared with respective initial rates of H_2O_2 production (Fig. 10). The linear relationship between surface areas and initial rates of H_2O_2 production observed in Fig. 10 indicates that the reactivity of each active site for water oxidation in the surface of $NiFe_2O_4$ remains unchanged irrespective of the particle size.

Conclusions

The reactivity of water oxidation catalysts for the photocatalytic production of H_2O_2 from H_2O and O_2 with $[Ru^{II}(Me_2phen)_3]^{2+}$ and Sc^{3+} was improved by using $[Ir(Cp*)(H_2O)_3]^{2+}$ as a precatalyst, which was converted to $Ir(OH)_3$ nanoparticles during the photocatalytic reaction, as compared with that using $Ir(OH)_3$ nanoparticles derived from H_2IrCl_6. The enhanced catalytic reactivity of $Ir(OH)_3$ nanoparticles results from the smaller size of nanoparticles produced *in situ* as compared with $Ir(OH)_3$ nanoparticles derived from H_2IrCl_6. The Cp* ligand of $[Ir(Cp*)(H_2O)_3]^{2+}$ was partially oxidised to CO_2 during the photocatalytic reaction and remaining organic residues may act as capping reagents to prevent further aggregation of $Ir(OH)_3$ nanoparticles. $NiFe_2O_4$ nanoparticles, which are composed of much more earth abundant metals than Ir, also acted as a water oxidation catalyst for the photocatalytic production of H_2O_2 with $[Ru^{II}(Me_2phen)_3]^{2+}$ in the presence of Sc^{3+} in water. In this case, the size of $NiFe_2O_4$ nanoparticles decreased during the photocatalytic reaction to increase the catalytic reactivity of water oxidation. Thus, both a bottom-up method starting from a metal complex precatalyst ($[Ir(Cp*)(H_2O)_3]^{2+}$) to produce $Ir(OH)_3$ nanoparticles with small size and a top-down method starting from as-prepared $NiFe_2O_4$ to obtain smaller $NiFe_2O_4$ nanoparticles provide promising strategies to develop more efficient water oxidation catalysts for photocatalytic production of H_2O_2 from H_2O and O_2.

Fig. 10 Plot of initial rates of the photocatalytic H_2O_2 production *vs.* ratios of the specific surface area (R) of $NiFe_2O_4$ particles, where R = (specific surface area of the particles)/(specific surface area of non-treated $NiFe_2O_4$). The details of the calculation are described in ESI (Page S23).† The circles denoted as 1–4 correspond to $NiFe_2O_4$ particles with diameters of 1300 nm, 620 nm, 120 nm and 91 nm, respectively. The methods to produce each size of $NiFe_2O_4$ particles and the calculation of initial H_2O_2 production rates are described in the caption of Fig. S17.†

Experimental section

Materials

All chemicals commercially available were used without further purification unless otherwise noted. $H_2IrCl_6 \cdot nH_2O$ (99.99%) was purchased from Furuya Metal. $RuCl_3$ (38.220 wt% Ru) was purchased from Tanaka Kikinzoku Kogyo K.K. 4,7-Dimethyl-

This journal is © The Royal Society of Chemistry 2015

J. Mater. Chem. A, 2015, **3**, 12404–12412 | **12409**

1,10-phenanthroline (Me$_2$phen, 98%), Ag$_2$SO$_4$ (99.9%) and (NH$_4$)$_2$SO$_4$ (99.99%) were supplied by Aldrich Chemicals. Pentamethylcyclopentadiene was obtained from Kanto Chemical Co., Inc. Oxo[5,10,15,20-tetra(4-pyridyl)porphinato]titanium(IV) ([TiO(tpyp)]) and NADH were supplied by Tokyo Chemical Industry Co., Ltd. (TCI). Sc(NO$_3$)$_3$·4H$_2$O (99.9%) was supplied by Mitsuwa Chemicals Co., Ltd. Purification of water (18.2 MΩ cm) was performed with a Milli-Q system (Millipore, Direct-Q 3 UV). [Ir(Cp*)(H$_2$O)$_3$]SO$_4$ was prepared by following the reported method.[68]

Synthesis of NiFe$_2$O$_4$

NiFe$_2$O$_4$ was synthesised according to the literature.[67,69] To an aqueous solution (24 mL) containing NiCl$_2$·6H$_2$O (2.0 mmol, 0.46 g) and Fe(NO$_3$)$_3$·9H$_2$O (4.0 mmol, 1.6 g) was added KOH solution (2.0 M, 24 mL) with magnetic stirring at room temperature (RT). The mixture was then transferred into a Teflon-lined stainless-steel autoclave of 140 mL capacity. The sealed tank was heated to and maintained at 160 °C for 10 h in an oven and cooled to RT. The resulting brown precipitates were collected by filtration and washed with water and ethanol more than 3 times, and finally dried in an oven at 60 °C for 10 h.

Formation of NiFe$_2$O$_4$ nanoparticles

Typically, an aqueous suspension (3.0 mL) containing Sc(NO$_3$)$_3$ and NiFe$_2$O$_4$ (0.50 mg) was stirred continuously for 3 h, 6 h or 12 h at 80 °C under room light to yield 220 nm, 120 nm and 91 nm nanoparticles respectively. The suspension was used for the H$_2$O$_2$ production reaction after the addition of [Ru^{II}(Me$_2$phen)$_3$]$^{2+}$ and Sc(NO$_3$)$_3$. NiFe$_2$O$_4$ nanoparticles used as a sample for powder XRD measurements were prepared by immersing as-prepared NiFe$_2$O$_4$ (5.1 mg) in an aqueous solution (31 mL) of Sc(NO$_3$)$_3$ for 12 h. The resulting powder was collected by centrifugation and washed with water 3 times. The yield of NiFe$_2$O$_4$ nanoparticles was 87%.

Quantitative measurements of Fe^{II} and Fe^{III} ions

An aqueous suspension containing as-prepared NiFe$_2$O$_4$ and Sc(NO$_3$)$_3$ was stirred at 80 °C for 12 h for the formation of active NiFe$_2$O$_4$ nanoparticles as discussed in the previous paragraph. After the formation of NiFe$_2$O$_4$ nanoparticles, the supernatant of the suspension was examined for the presence of Fe^{II} or Fe^{III} ions. The filtered supernatant was diluted by water so that the solution may contain 300 μM of Fe ions if NiFe$_2$O$_4$ was dissolved completely. UV-Vis spectra were measured using a Hewlett Packard 8453 diode array spectrometer for the diluted supernatant in both the presence of 1,10-phenanthroline (phen) (4.5 mM), and in the presence of phen (4.5 mM) and NADH (1.5 mM) to reduce Fe^{III} that may have formed. Measured UV-Vis spectra were compared with the UV-Vis spectra of [Fe^{II}(phen)$_3$]$_3$$^{2+}$ (100 μM).

Photocatalytic reactions

[Ir(Cp*)(H$_2$O)$_3$]SO$_4$ or NiFe$_2$O$_4$ was introduced into distilled water (3.0 mL) containing [Ru^{II}(Me$_2$phen)$_3$]SO$_4$ and Sc(NO$_3$)$_3$ in a quartz cuvette with a light path length of 1.0 cm. The solution was bubbled with oxygen gas for ∼30 min. The solution containing photocatalyst was irradiated with a xenon lamp (USHIO Optical Modulex SX-UID 501XAMQ) through a cut-off filter (Asahi Techno Glass L42) transmitting $\lambda > 420$ nm at room temperature.

Quantification of produced H$_2$O$_2$

From spectroscopic titration with an acidic solution of the [TiO(tpypH$_4$)]$^{4+}$ complex (Ti-TPyP reagent), the amount of produced H$_2$O$_2$ was determined.[70] The [TiO(tpyp)] complex (34 mg) was dissolved in 1.0 L of 50 mM hydrochloric acid and the solution was used as a Ti-TPyP reagent. An aliquot (*e.g.*, 100 μL) of the reaction solution was diluted with water and 0.25 mL of the sample solution was mixed with 0.25 mL of 4.8 M perchloric acid and 0.25 mL of Ti-TPyP reagent. After 5 min at room temperature, the mixture was diluted to 2.5 mL with water and used for the spectroscopic measurement. The absorbance at $\lambda = 434$ nm was measured by using a Hewlett Packard 8453 diode array spectrometer (A_S). In a similar manner, a blank solution was prepared by adding distilled water in place of the sample solution in the same volume with its absorbance designated as A_B. The difference in absorbance was determined by following the equation: $\Delta A_{434} = A_B - A_S$. Based on ΔA_{434} and the volume of the solution, the amount of hydrogen peroxide was determined according to the literature.[70]

Determination of the quantum yield

Quantum yields (QYs) of the photocatalytic production of hydrogen peroxide (Φ) were determined under irradiation of monochromatised light using a Shimadzu spectrofluorophotometer (RF-5300 PC) through a monochromator transmitting $\lambda = 450$ nm, and estimated as

$$QY \ (\%) = (2 \times R/I) \times 100 \tag{4}$$

where R (mol s^{-1}) and I (einstein s^{-1}) represent the H$_2$O$_2$ production rate and the light intensity, respectively. Two photons are required for the electronic transition of the [Ru^{II}(Me$_2$phen)$_3$]$^{2+}$ photosensitiser in order to produce hydrogen peroxide through two-electron reduction of one molecule of oxygen. When all of the photons are fully utilized to produce hydrogen peroxide, the QY reaches 100%. Therefore, the coefficient of the right-hand side in eqn (4) is 2 for this photocatalytic system. The total number of incident photons was measured by a standard method using an actinometer and potassium ferrioxalate, K$_3$[Fe^{III}(C$_2$O$_4$)$_3$], in H$_2$O at room temperature under photoirradiation using a Shimadzu spectrofluorophotometer (RF-5300 PC) through a monochromator transmitting $\lambda = 450$ nm (slit width of 5.0 mm) at room temperature. For the same quartz cuvette with a light path length of 1.0 cm with 3.0 mL solution as used in the production of hydrogen peroxide experiments, the rate of photon flux of the incident light (I) was determined to be 7.40×10^{-10} einstein s^{-1}.

12410 | *J. Mater. Chem. A*, 2015, **3**, 12404–12412

This journal is © The Royal Society of Chemistry 2015

Quantification of evolved CO₂

[Ir(Cp*)(H₂O)₃]SO₄ (100 μM) was added to distilled water (3.0 mL) containing [Ru^{II}(Me₂phen)₃]SO₄ (20 μM) and Sc(NO₃)₃ (100 mM) in a quartz cuvette (light path length = 1.0 cm). The solution was saturated by bubbling with oxygen gas for ∼30 min. The photocatalyst was irradiated with a xenon lamp (USHIO Optical Modulex SX-UID 501XAMQ) through a cut-off filter (Asahi Techno Glass L42) transmitting λ > 420 nm at room temperature. The amount of evolved CO₂ was determined by using a Shimadzu GC-14B gas chromatograph (N₂ carrier, active carbon with a particle size of 60–80 mesh at 80 °C) equipped with a TCD detector.

Characterisation of particles

Transmission electron microscopy (TEM) images of iridium hydroxide and nickel ferrite, which were mounted on a copper microgrid coated with elastic carbon, were observed using a JEOL JEM-2100 operating at 200 kV. Dynamic light scattering (DLS) data were obtained using a Zeta Sizer Nano ZS (Malvern Instruments Ltd., USA). Powder X-ray diffraction (XRD) patterns were recorded with a Rigaku MiniFlex 600 X-ray diffractometer. X-ray photoelectron spectra (XPS) were obtained with an ULVAC-PHI ESCA5600 X-ray photoelectron spectrophotometer. The incident radiation was the Mg Kα X-ray (1253.6 eV) at 400 W and the charge neutralizer was turned on for acquisition. The binding energy of each element was corrected by the C 1s peak (284.8 eV) from residual carbon.

Acknowledgements

Notes and references

1 J. A. Herron, J. Kim, A. A. Upadhye, G. W. Huber and C. T. Maravelias, *Energy Environ. Sci.*, 2015, **8**, 126.

2 J. R. McKone, N. S. Lewis and H. B. Gray, *Chem. Mater.*, 2014, **26**, 407.

3 T. A. Faunce, W. Lubitz, A. W. Rutherford, D. MacFarlane, G. F. Moore, P. Yang, D. G. Nocera, T. A. Moore, D. H. Gregory, S. Fukuzumi, K. B. Yoon, F. A. Armstrong, M. R. Wasielewski and S. Styring, *Energy Environ. Sci.*, 2013, **6**, 695.

4 S. Fukuzumi, D. Hong and Y. Yamada, *J. Phys. Chem. Lett.*, 2013, **4**, 3458.

5 S. Fukuzumi and Y. Yamada, *ChemSusChem*, 2013, **6**, 1834.

6 J. M. Thomas, *Energy Environ. Sci.*, 2014, **7**, 19.

7 *Hydrogen as a Future Energy Carrier*, ed. A. Züttel, A. Borgschulte and L. Schlapbach, Wiley-VCH, Weinheim, 2008.

8 Q. Jia, A. Iwase and A. Kudo, *Chem. Sci.*, 2014, **5**, 1513.

9 M. G. Walter, E. L. Warren, J. R. McKone, S. W. Boettcher, Q. Mi, E. A. Santori and N. S. Lewis, *Chem. Rev.*, 2010, **110**, 6446.

10 K. Maeda and K. Domen, *J. Phys. Chem. Lett.*, 2010, **1**, 2655.

11 X. Chen, S. Shen, L. Guo and S. S. Mao, *Chem. Rev.*, 2010, **110**, 6503.

12 K. Maeda, K. Teramura, D. Lu, T. Takata, N. Saito, Y. Inoue and K. Domen, *Nature*, 2006, **440**, 295.

13 M. D. Symes and L. Cronin, *Nat. Chem.*, 2013, **5**, 403.

14 S. Fukuzumi and T. Suenobu, *Dalton Trans.*, 2013, 18.

15 Y. Maenaka, T. Suenobu and S. Fukuzumi, *Energy Environ. Sci.*, 2012, **5**, 7360.

16 S. Fukuzumi, Y. Yamada and K. D. Karlin, *Electrochim. Acta*, 2012, **82**, 493.

17 S. Fukuzumi and Y. Yamada, *Aust. J. Chem.*, 2014, **67**, 354.

18 Y. Yamada, M. Yoneda and S. Fukuzumi, *Inorg. Chem.*, 2014, **53**, 1272.

19 S. Yamazaki, Z. Siroma, H. Senoh, T. Ioroi, N. Fujiwara and K. Yasuda, *J. Power Sources*, 2008, **178**, 20.

20 S. A. M. Shaegh, N.-T. Nguyen, S. M. M. Ehteshami and S. H. Chan, *Energy Environ. Sci.*, 2012, **5**, 8225.

21 F. Yang, K. Cheng, X. Xiao, J. Yin, G. Wang and D. Cao, *J. Power Sources*, 2014, **245**, 89.

22 Y. Yamada, M. Yoneda and S. Fukuzumi, *Chem.–Eur. J.*, 2013, **19**, 11733.

23 Y. Yamada, Y. Fukunishi, S. Yamazaki and S. Fukuzumi, *Chem. Commun.*, 2010, **46**, 7334.

24 S. Kato, J. Jung, T. Suenobu and S. Fukuzumi, *Energy Environ. Sci.*, 2013, **6**, 3756.

25 C. J. Gagliardi, A. K. Vannucci, J. J. Concepcion, Z. Chen and T. J. Meyer, *Energy Environ. Sci.*, 2012, **5**, 7704.

26 D. J. Wasylenko, R. D. Palmer and C. P. Berlinguette, *Chem. Commun.*, 2013, **49**, 218.

27 X. Liu and F. Wang, *Coord. Chem. Rev.*, 2012, **256**, 1115.

28 R. Cao, W. Lai and P. Du, *Energy Environ. Sci.*, 2012, **5**, 8134.

29 A. Singh and L. Spiccia, *Coord. Chem. Rev.*, 2013, **257**, 2607.

30 C. W. Cady, R. H. Crabtree and G. W. Brudvig, *Coord. Chem. Rev.*, 2008, **252**, 444.

31 M.-T. Zhang, Z. Chen, P. Kang and T. J. Meyer, *J. Am. Chem. Soc.*, 2013, **135**, 2048.

32 Y. Jiang, F. Li, B. Zhang, X. Li, X. Wang, F. Huang and L. Sun, *Angew. Chem., Int. Ed.*, 2013, **52**, 3398.

33 M. Murakami, D. Hong, T. Suenobu and S. Fukuzumi, *J. Am. Chem. Soc.*, 2011, **133**, 11605.

34 Q. S. Yin, J. M. Tan, C. Besson, Y. V. Geletii, D. G. Musaev, A. E. Kuznetsov, Z. Luo, K. I. Hardcastle and C. L. Hill, *Science*, 2010, **328**, 342.

35 J. L. Fillol, Z. Codolà, I. Garcia-Bosch, L. Gómez, J. J. Pla and M. Costas, *Nat. Chem.*, 2011, **3**, 807.

36 D. Hong, S. Mandal, Y. Yamada, Y.-M. Lee, W. Nam, A. Llobet and S. Fukuzumi, *Inorg. Chem.*, 2013, **52**, 9522.

37 G. Chen, L. Chen, S.-M. Ng, W.-L. Man and T.-C. Lau, *Angew. Chem., Int. Ed.*, 2013, **52**, 1789.

This journal is © The Royal Society of Chemistry 2015

J. Mater. Chem. A, 2015, **3**, 12404–12412 | 12411

38 Y. Liu, S.-M. Ng, S.-M. Yiu, W. W. Y. Lam, X.-G. Wei, K.-C. Lau and T.-C. Lau, *Angew. Chem., Int. Ed.*, 2014, **53**, 14468.

39 T. Zhang and W. Lin, *Chem. Soc. Rev.*, 2014, **43**, 5982.

40 S. Berardi, S. Drouet, L. Francas, C. Gimbert-Surinach, M. Guttentag, C. Richmond, T. Stoll and A. Llobet, *Chem. Soc. Rev.*, 2014, **43**, 7501.

41 M. Hirahara, A. Shoji and M. Yagi, *Eur. J. Inorg. Chem.*, 2014, 595.

42 M. D. Kärkäs, E. V. Johnston, O. Verho and B. Åkermark, *Acc. Chem. Res.*, 2014, **47**, 100.

43 A. R. Parent and K. Sakai, *ChemSusChem*, 2014, **7**, 2070.

44 X. Sala, S. Maji, R. Bofill, J. Garcia-Anton, L. Escriche and A. Llobet, *Acc. Chem. Res.*, 2014, **47**, 504.

45 J. J. Stracke and R. G. Finke, *ACS Catal.*, 2014, **4**, 909.

46 N. D. McDaniel, F. J. Coughlin, L. L. Tinker and S. Bernhard, *J. Am. Chem. Soc.*, 2008, **130**, 210.

47 J. F. Hull, D. Balcells, J. D. Blakemore, C. D. Incarvito, O. Eisenstein, G. W. Brudvig and R. H. Crabtree, *J. Am. Chem. Soc.*, 2009, **131**, 8730.

48 J. D. Blakemore, N. D. Schley, D. Balcells, J. F. Hull, G. W. Olack, C. D. Incarvito, O. Eisenstein, G. W. Brudvig and R. H. Crabtree, *J. Am. Chem. Soc.*, 2010, **132**, 16017.

49 D. G. H. Hetterscheid and J. N. H. Reek, *Chem. Commun.*, 2011, **47**, 2712.

50 J. D. Blakemore, N. D. Schley, G. W. Olack, C. D. Incarvito, G. W. Brudvig and R. H. Crabtree, *Chem. Sci.*, 2011, **2**, 94.

51 N. D. Schley, J. D. Blackmore, N. K. Subbaiyan, C. D. Incarvito, F. D'Souza, R. H. Crabtree and G. W. Brudvig, *J. Am. Chem. Soc.*, 2011, **133**, 10473.

52 D. B. Grotjahn, D. B. Brown, J. K. Martin, D. C. Marelius, M.-C. Abadjian, H. N. Tran, G. Kalyuzhny, K. S. Vecchio, Z. G. Specht, S. A. Cortes-Llamas, V. Miranda-Soto, C. van Niekerk, C. E. Moore and A. L. Rheingold, *J. Am. Chem. Soc.*, 2011, **133**, 19024.

53 U. Hintermair, S. W. Sheehan, A. R. Parent, D. H. Ess, D. T. Richens, P. H. Vaccaro, G. W. Brudvig and R. H. Crabtree, *J. Am. Chem. Soc.*, 2013, **135**, 10837.

54 D. Hong, M. Murakami, Y. Yamada and S. Fukuzumi, *Energy Environ. Sci.*, 2012, **5**, 5708.

55 G. S. Nahor, P. Hapiot, P. Neta and A. Harriman, *J. Phys. Chem.*, 1991, **95**, 616.

56 T. Nakagawa, N. S. Bjorge and R. W. Murray, *J. Am. Chem. Soc.*, 2009, **131**, 15578.

57 Y. Zhao, E. A. Hernandez-Pagan, N. M. Vargas-Barbosa, J. L. Dysart and T. E. Mallouk, *J. Phys. Chem. Lett.*, 2011, **2**, 402.

58 A. Harriman, I. J. Pickering, J. M. Thomas and P. A. Christensen, *J. Chem. Soc., Faraday Trans. 1*, 1988, **84**, 2795.

59 F. Jiao and H. Frei, *Energy Environ. Sci.*, 2010, **3**, 1018.

60 N. D. Morris and T. E. Mallouk, *J. Am. Chem. Soc.*, 2002, **124**, 11114.

61 S. Fukuzumi and D. Hong, *Eur. J. Inorg. Chem.*, 2014, **4**, 645.

62 G. Q. Wei, Y. X. Wang, C. D. Huang, Q. J. Gao, Z. T. Wang and L. Xu, *Int. J. Hydrogen Energy*, 2010, **35**, 3951.

63 M. W. Kanan and D. G. Nocera, *Science*, 2008, **321**, 1072.

64 D. J. Wasylenko, R. D. Palmer, E. Schott and C. P. Berlinguette, *Chem. Commun.*, 2012, **48**, 2107.

65 M. Hara, K. Asami, K. Hashimoto and T. Masumoto, *Electrochim. Acta*, 1983, **28**, 1073.

66 H. Y. Hall and P. M. A. Sherwood, *J. Chem. Soc., Faraday Trans. 1*, 1984, **80**, 135.

67 D. Hong, Y. Yamada, T. Nagatomi, Y. Takai and S. Fukuzumi, *J. Am. Chem. Soc.*, 2012, **134**, 19572.

68 S. Ogo, N. Makihara and Y. Watanabe, *Organometallics*, 1999, **18**, 5470.

69 Y. Cheng, Y. Zheng, Y. Wang, F. Bao and Y. J. Qin, *Solid State Chem.*, 2005, **178**, 2394.

70 C. Matsubara, N. Kawamoto and K. Takamura, *Analyst*, 1992, **117**, 1781.

12412 | *J. Mater. Chem. A*, 2015, **3**, 12404–12412

This journal is © The Royal Society of Chemistry 2015